RSC Advances

ROYAL SOCIETY OF CHEMISTRY

www.rsc.org/advances

Carbon Dioxide Hydrogenation to Methanol over Cu-ZrO_2/CNTs: Effect of Carbon Surface Chemistry

Guannan Wang,[a] Limin Chen,*[a,b] Yuhai Sun,[a] Junliang Wu,[a] Mingli Fu,[a] Daiqi Ye*[a,b]

[a] *G.N. Wang, Prof. Dr. L.M. Chen, Y.H. Sun, Prof. Dr. J.L. Wu, Prof. Dr. M.L. Fu, Prof. Dr. D.Q. Ye, School of Environment and Energy, South China University of Technology, Guangzhou Higher Education Mega Centre, Guangzhou 510006, PR China. E-mail address: liminchen@scut.edu.cn (L.M. Chen), cedqye@scut.edu.cn (D.Q. Ye); Tel: 86-20-*39389592.

[b] *Prof. Dr. L.M. Chen, Prof. Dr. D.Q. Ye, Guangdong Provincial Key Laboratory of Atmospheric Environment and Pollution Control, South China University of Technology, Guangzhou Higher Education Mega Centre, Guangzhou 510006, PR China*

Abstract

Methanol synthesis from CO_2 hydrogenation in a fixed-bed plug flow reactor was investigated over Cu-ZrO_2 catalysts supported on CNTs bearing various functional groups. The highest methanol activity (turnover frequency $1.61x10^{-2}$ s^{-1}, space time yield 84.0 $mg \cdot g^{-1}_{(cat)} \cdot h^{-1}$) was obtained over Cu-$ZrO_2$/CNTs catalyst (CZ/CNT-3) with CNTs functionalized by nitrogen-containing groups and Cu loading only about 10.3 wt% under the reaction conditions of 260 °C, 3.0 MPa, $V(H_2):V(CO_2):V(N_2)$ = 69:23:8 and GHSV of 3600 h^{-1}. The catalysts were full characterized by N_2 physisorption, X-ray photoelectron spectroscopy (XPS), X-ray diffraction (XRD), H_2-temperature-programmed reduction (H_2-TPR) and temperature-programmed desorption of H_2 (H_2-TPD) techniques. The excellent performance of CZ/CNT-3 is attributed to the presence of nitrogen-containing groups on the CNTs surface, which increase the dispersion of copper oxides, promote their reduction, decreases the crystal size of Cu, enhances H_2 and CO_2 adsorption capability, thus leading to the good catalytic performance towards methanol synthesis.

Keywords: CO_2 hydrogenation; Methanol synthesis; Carbon nanotubes; Surface functional groups; Renewable resources

Introduction

CO_2 emission issue is getting more and more sophisticated because it is not only an environmental problem but also becoming an economical and political one. Thus, reducing CO_2 emission is becoming more and more urgent. Recently, the intergovernmental Panel on Climate Change (IPCC) has announced that the rising fossil fuel burning and deforestation are responsible for CO_2 concentration increasing from pre-industrial (prior to 1750) levels of 280 ppm to 400 ppm today.[1] It is generally accepted that the conversion of CO_2 to fuels can reduce CO_2 emission efficiently and, simultaneously, alleviate our dependence on fossil energy.[1-7] CO_2 conversion to methanol has been recognized as one of the most promising and effective technology due to its indispensable position in chemical industry and renewable energy field.[1,8,9] In chemical industry, the prominent role of methanol has been extensively reviewed in *methanol economy* written by Nobel Laureate Olah et al.[10] In renewable energy, methanol is not only served as one of the most important fuel alternatives but also as one of the most significant energy storage medium due to its high energy density by both volume and weight as well as many other advantages in comparison with compressed air, flywheels, batteries, supercapacitors etc.[1] Therefore, the research of CO_2 conversion to methanol is experiencing a renaissance.[11-16] Compared with renewable energy-based direct CO_2 conversion to methanol, i.e. artificial photosynthesis, photoelectrochemical reduction, electrochemical reduction etc., thermochemical routes are considered as the practical one.[1,5,6]

Various catalytic systems have been employed for methanol synthesis from CO_2 by catalytic hydrogenation (thermochemical) routes. Among them, Cu/ZnO and Cu/ZrO_2 based catalysts are the most commonly used ones. Cu/ZrO_2 catalyst was widely investigated due to its high stability and selectivity to methanol.[17-18] In contrast to the methanol production from synthesis gas, an equivalent amount of H_2O generates during the process of CO_2 hydrogenation. Large amount of H_2O can not only decrease methanol yield, but also accelerate the crystallization of Cu and ZrO_2, which usually deactivates the catalysts rapidly.[17-18] Carbon materials have strong hydrophobicity and can prompt the H_2O desorption from the surface soon after its formation. Therefore, carbon materials can reduce the negative effects of H_2O and are desirable support of the catalysts.[19-22]

Carbon nanotubes (CNTs) are usually used as catalyst support for CO and CO_2 hydrogenation due to their high aspect ratio (length/diameter), specific surface area, mechanical strength, rigidity, electric conductivity, thermostability and adjustable surface chemistry.[20-24] Bao et al.[23,24] extensively investigated the confinement effects of CNTs and revealed that the catalysts, such as FeN, confined in the channel of CNTs are more active for CO hydrogenation than the catalysts dispersed on the CNT exterior walls. Zhang et al.[20,21] reported that the activity and alcohol selectivity in CO/CO_2 hydrogenation was remarkably improved over metal decorated CNTs promoted $Cu\text{-}ZnO\text{-}Al_2O_3$ oxide and Co-Cu catalysts. The same group also developed highly active Pd-ZnO/CNTs catalyst for CO_2 hydrogenation to methanol.[22] Their research demonstrated that the ‘‘Herringbone-type (h-type)’’ CNTs supported

Pd-ZnO catalyst is more active than ‘‘Parallel-type (p-type)’’ CNTs supported one.[22] This means the structure of CNTs plays important roles in CO_2 hydrogenation to methanol.

Besides, carbon surface chemistry also plays vital roles on the catalytic properties.[25-27] Our previous research demonstrated that carbon surface chemistry can influence catalyst particle size and support-metal interactions remarkably, then modify the catalytic performance dramatically, especially for multi-component catalytic systems. The similar phenomena were also reported by other researchers.[28-31] In general, carbon surface can prompt H_2O desorption due to its high hydrophobicity; when functionalized with basic groups, it should further benefit to CO_2 adsorption as well as H_2 adsorption due to the highly dispersed catalyst formation. Therefore, in this research, Cu-ZrO_2 catalysts supported on CNTs functionalized with various surface groups, such as nitrogen-containing groups (basic), oxygen-containing groups (acidic), and few oxygen-containing groups (close to neutral) were investigated to elucidate the effects of carbon surface chemistry on the catalytic properties of CO_2 hydrogenation to methanol.

Experimental

Catalyst preparation

In this work, CNTs supports with different surface functional groups were selected to prepare the supported Cu-ZrO_2 catalysts. Two types of multi-walled carbon nanotubes (original CNTs and nitrogen containing CNTs) with outer diameters of 8-15 nm were supplied by Chengdu Institute of Organic Chemistry. Original CNTs

were put in 68 wt% HNO_3 at 140 ℃ for 14 h in an oil bath, and then the mixture was filtered and washed with de-ionized water, followed by drying at 100 °C overnight. The obtained sample was designed as CNTs-1. CNTs-1 was further calcined in N_2 stream at 600 ℃ for 6 h, the obtained sample was marked as CNTs-2. Nitrogen containing CNTs was used directly without further purification and labeled as CNTs-3.

The $Cu/ZrO_2/CNTs$ catalysts were prepared using a deposition-precipitation method and the mass ratio was 10/40/50 for $Cu/ZrO_2/CNTs$. The process was as the following: A mixed aqueous solution containing calculated amounts of $Cu(NO_3)_2{\cdot}3H_2O$ (AR grade, Guangzhou Chemical Reagent Factory) and $ZrO(NO_3)_2$ (AR grade, Shanghai Aladdin), as well as the pre-determined amount of precipitant NaOH (0.2 $mol{\cdot}L^{-1}$, AR grade, Sinopharm Chemical Reagent Co. Ltd.) aqueous solution were simultaneously dropped into the glass container which contained a calculated amount of the CNTs dispersion in water. The suspension was stirred vigorously at 70 ^oC, in order to maintain the pH value in the range of 7.0-7.5. After precipitation, the solid was kept at 70 ^oC for another 30 min under stirring, and then aged at room temperature for 1 h. The obtained solid was washed with de-ionized water and finally recovered by filtration. This process was repeated several times until the pH of the filtrate was 7.0±0.2. The solid was subsequently dried at 100 ℃ overnight, calcined in pure N_2 at 350 ℃ for 2 h in a tube furnace. The catalysts with different CNTs supports were named as the CZ/CNTs-1, CZ/CNTs-2, CZ/CNTs-3, respectively.

Catalyst characterization

X-ray photoelectron spectroscopy (XPS) measurements were conducted on an ESCALAB 250 spectrometer (Thermo Fisher Scientific) equipped with Mg Kα radiation (hυ = 1253.6 eV). The energy resolution was 0.45 eV, the imaging spatial resolution was 3 μm and the minimum analysis area was 15 μm. C1s binding energy corresponding to graphitic carbon was set at 284.6 eV and used as reference to position the other peaks. Fitting of the XPS spectra was essential for the determination of the relative amount of oxygen functionalized carbon species on the surface by using XPS PEAK4.1 software.

The specific surface area, pore volume and pore size were determined by N_2 adsorption/desorption isotherms at -196 ℃, using an ASAP 2020N Accelerated Surface Area and Porosimetry system (Micromeritics Instrument Corp). Before the analysis, all samples were degassed under vacuum at 300 ℃ for 4 h. The specific surface area and pore size distribution were determined according to five point test formula and BJH method, respectively.

The actual composition of metal elements in the catalysts was measured using an OPTIMA 8000DV ICP-AES (Perkin-Elmer). A sample with 20 mg was pretreated by nitrohydrochloric acid at 160 ℃ for 10 h.

X-ray diffraction (XRD) analysis were recorded on a D8 Advance X-ray diffractometer (Bruker) with Cu Kα radiation (λ = 0.15418 nm, 40 kV, 40 mA) in the 2θ range of 10-90°. The XRD results were analyzed by comparison with JCPDS cards.

Temperature-programmed reduction in H_2 (H_2-TPR) was carried out with Micromeritics AutoChem II2920 instrument in a quartz U-tube reactor. Prior to the reduction, the sample (ca. 100 mg) was pretreated in flowing Ar stream at 300 ℃ for 30 min and then cooled down to 60 ℃. Afterwards, a 10 vol.% H_2/Ar flow (30 $mL \cdot min^{-1}$) was passed over the sample at a heating rate of 10 $℃ \cdot min^{-1}$ from 60 to 800 ℃. The hydrogen consumption was monitored by a TCD quantitatively calibrated with a commercial CuO standard.

Temperature-programmed H_2 desorption (H_2-TPD) was performed at Micromeritics AutoChem II2920 system. The sample was first reduced in 5 vol% H_2/Ar at 30 $mL \cdot min^{-1}$ at 240 ℃ for 6 h. After cooling down to 60 ℃ in He, the catalyst was saturated with H_2 in 10 vol% H_2/Ar at a rate of 30 $mL \cdot min^{-1}$ for 60 min and then flushed with He flow at 30 $mL \cdot min^{-1}$ to remove all physical adsorbed molecules. Afterward, the TPD experiment was started with a heating rate of 5 $℃ \cdot min^{-1}$ to 650 ℃ under He flow at 30 $mL \cdot min^{-1}$. The desorbed H_2 was detected by an on-line TCD. Temperature-programmed CO_2 desorption (CO_2-TPD) was similar to that of H_2-TPD, except that the catalyst was saturated with CO_2 in 80 vol% CO_2/Ar and TPD experiment was conducted under Ar flow.

Catalyst Evaluation

CO_2 hydrogenation to methanol was tested in a continuous-flow, high pressure, fixed-bed reactor. Catalyst (500 mg) was placed in the center of a stainless steel tube reactor and the other part was filled with quartz sand (40-60 mesh). Prior to the reaction, the catalyst was calcinated in N_2 at 350 ℃ for 2 h, then reduced in situ in 5

vol% H_2/Ar at 240 °C for 10 h. The reaction was conducted at a stationary state under reaction conditions of 200-300 °C, 3.0 MPa, $V(H_2):V(CO_2):V(N_2)$ = 69:23:8 and GHSV = 3600 $mL \cdot g_{cat}^{-1} \cdot h^{-1}$. The product mixtures were analyzed by an on-line gas chromatograph (Model 2014C for Shimazu) equipped with dual detectors (TCD and FID) and triplet columns. The TCD detector was equipped with 5A column and PQ column (3.0 m length), used for the analysis of N_2 (internal standard), CO and CO_2; the FID detector was equipped with a capillary column of 30.0 m long, used for the analysis of CH_3OH, CH_4, C_2H_6 and CH_3OCH_3. CO_2 conversion was calculated by a N_2 internal standard analysis method. The carbon-based selectivity for the hydrogenation products, CH_3OH, CO and hydrocarbons was calculated by an internal normalization method. The specific calculation method can be found in the reference.[22] The TOF calculation was based on the diameter of Cu which was calculated by Scherrer equation through XRD results. TOF was calculated through the following equation:

$$TOF = \mu_{CO2} \cdot X_{CO2} \cdot M_{Cu} / (Vm \cdot w_{Cu} \cdot m_{cat} \cdot D_{Cu})$$

Where μ_{CO2} is CO_2 flow rate in the feed gas, X_{CO2} is CO_2 conversion, M_{Cu} is molar mass of Cu, Vm is standard molar volume of gas, w_{Cu} is mass percent of Cu, m_{cat} is catalyst mass, D_{Cu} is the dispersion of Cu, calculated through the diameter of Cu[32].

Results and Discussion

Catalyst Performance

All catalysts were prepared using deposition-precipitation method with the initial mass ratio of 10/40/50 for $Cu/ZrO_2/CNTs$. $Cu\text{-}ZrO_2/CNTs$ with the CNTs bearing oxygen-, few oxygen- and nitrogen-containing groups were denoted as CZ/CNTs-1, CZ/CNTs-2 and CZ/CNTs-3, respectively. Their catalytic properties for CO_2 hydrogenation to methanol are displayed in Figure 1. As shown, both CO_2 conversion and CO selectivity increase with the reaction temperature, while CH_3OH selectivity decreases with the increase of reaction temperature. CH_3OH yield exhibits a volcano trend with temperature increase, and the maximum appears at 260 °C for all of the catalysts. Interestingly, all catalysts present similar CO_2 conversion, CH_3OH selectivity and CO selectivity when the reaction temperature is above 260 °C. This is mainly because CO_2 hydrogenation to methanol is an exothermic reversible reaction and it is close to equilibrium at high reaction temperatures. In sharp contrast, when the reaction temperature below 260 °C, CO_2 conversion, CH_3OH selectivity and CH_3OH yield over the investigated catalysts follow the same decrease order: CZ/CNTs-3 > CZ/CNTs-2 > CZ/CNTs-1. The highest CH_3OH yield was obtained over CZ/CNTs-3, about 7.07%, which is about 34.7% and 18.4% higher than that of CZ/CNTs-1 and CZ/CNTs-2, respectively. For comparison, the catalytic performance of 10 *wt*% Cu/ZrO_2 catalyst was also evaluated and presented in supporting information (Figure S-1). It exhibits similar catalytic properties to CZ/CNTs catalysts but with evidently lower CH_3OH yield. The stability of CZ/CNTs-3 was also tested at 260 °C, 3.0 MPa and the GHSV of 3600 $mL \cdot g_{cat}^{-1} \cdot h^{-1}$, as displayed in Figure 2. It is clear that the catalyst was slightly deactivated in the first 24 hours and then the catalytic

performance was retained in the following test time. This indicates that the introduction of CNTs indeed contributes to the catalyst stability.

In order to outstand the influence of CNTs on the catalytic performance, the turnover-frequency (TOF, the number of CO_2-molecule hydrogenated on unit site of exposed Cu per second, s^{-1}) and space time yield of methanol (STY, methanol yield per gram catalyst per hour, $mg \cdot g^{-1} \cdot h^{-1}$) are calculated and also listed in table 1. The TOF calculation was based on the particle size of Cu which was determined by XRD results (the dispersion of Cu, $D_{Cu} = 1/d_{Cu}$). The catalytic performance of other Cu-ZrO_2 containing systems are also collected from the literature and listed in Table 1 for comparison.[32-40] The data (Table 1) show that, both TOF and STY values of the investigated catalysts increase along the reaction temperature. At the same reaction temperature, the TOF closely resembles each other except that of CZ/CNTs-3 at 220 °C; however, the STY value increases in the order of CZ/CNTs-1, CZ/CNTs-2 and CZ/CNTs-3. This suggests the high methanol yield may originate from large amount of active sites at high reaction temperature. Due to the complexity of the catalyst composition and the shortage of reaction data, many efforts have been made to compare the current data with published ones in Table 1. The preliminary conclusions can be drawn that the TOF of the most active catalyst in the current research, CZ/CNTs-3, is obviously higher than most of those in the literature, accompanied with comparably high STY value with less copper mass (10.3 *wt*%). Although there are some catalytic systems, such as $Cu_{(58.6)}/ZrO_{2(41.4)}$, $Cu_{(27)}/B_2O_{3(3)}/ZrO_{2(70)}$, $Cu_{(27)}/Ga_2O_{3(3)}/ZrO_{2(70)}$ and $CuO_{(43)}/ZnO_{(17.4)}/ZrO_{2(39.6)}$, exhibit

higher STY value than the investigated catalysts, it may be due to the paramount high Cu loading, or the promotion effects of the third components and/or different catalyst preparation methods. The study indicates that CZ/CNTs behaviors remarkably high intrinsic CO_2 hydrogenation activity. The origination of high catalytic activity and STY values of the investigated catalysts will be discussed in details below.

Catalyst characterization

The surface chemistry of various CNTs samples was investigated by XPS. High-resolution XPS C1s region deconvolution of all samples was carried out, as shown in Figure 3. The C1s spectra can be resolved into C-C groups (BE = 284.6 eV), C=C groups (BE = 285.2-285.5 eV), C-OH groups (BE = 285.9-286.5 eV), C-N groups (BE = 286.7 eV), C=O groups (BE = 287.4-288.0 eV), COOH groups (BE = 289.0 eV) and shake-up satellite peaks due to $\pi \rightarrow \pi^*$ transitions in aromatic rings (BE > 290eV).[28-29] The calculated percentages of different types of carbon as well as carbon, oxygen and nitrogen content are listed in Table 2. It is very clear that CNTs-1 has the highest amount of oxygen about 7.03%; CNTs-2 holds the lowest amount about 1.89%; CNTs-3 possess the moderate amount of oxygen about 5.76%. Compared with CNTs-2, CNTs-1 has slightly higher amount of C-OH, C=O and COOH groups, especially less stable acidic COOH groups; moreover, it is negligible over CNTs-2. This means heat treatment in inert atmosphere at high temperature removes large amount of oxygen containing functional groups, especially less stable acidic COOH groups. This suggests that it is possible to reveal the influence of oxygen containing functional groups, especially COOH groups on the catalytic

properties. In addition, compared with CNTs-1, CNTs-3 has nearly similar amount of stable C-OH, C=O groups and less stable acidic COOH groups; therefore, it enables the investigation of the effect of nitrogen-containing functional groups on the catalytic properties. The deconvolution of XPS O1s spectra were also conducted and put in supporting information (Figure S-2 and Table S-3). The results are in accordance with C1s spectra.

In order to obtain clear information of nitrogen-containing groups on CNTs-3, the deconvolution of N1s peak was conducted and displayed in Figure 4. According to the previous publications, there are three types of nitrogen-containing functional groups on the surface of CNTs-3.[30] The most abundant one is ascribed to pyridinic-type nitrogen with BE = 398.2 eV; the moderate abundance one is attributed to various forms of quaternary nitrogen atoms with BE = 400.8 eV; the least one is assigned to oxygenated nitrogen species with BE = 402.7 eV.[30] All of these groups are basic and prone to combine with catalyst precursors and adsorb acidic CO_2. However, their interactions with the catalyst precursors and adsorption strength/capacity are quite different; furthermore, it is difficult to distinguish their functions from each other. Thus, the total effects of basic nitrogen-containing groups on the catalytic properties will be investigated.

The specific surface area, pore volume and pore size distribution of various CNTs and the corresponding catalysts after calcination are listed in Table 3. It is found that the specific surface area for CNTs-2 (193 $m^2 \cdot g^{-1}$) is obviously higher, compared to the other two analogs (184 $m^2 \cdot g^{-1}$and 160 $m^2 \cdot g^{-1}$ for CNTs-1 and CNTs-3,

respectively). The pore volume of three CNTs does the same trend. Furthermore, after loading metal, both surface area and pore volume of CZ/CNTs catalysts decreased, accompanied with limited pore size decrease. The actual components of the catalysts is measured by ICP-AES and also listed in Table 3. It can be seen that the Cu loadings are 12.8%, 12.3% and 10.3 wt% for CZ/CNTs-1, CZ/CNTs-2 and CZ/CNTs-3, respectively (Table 3). The obviously lower loadings of Cu and ZrO_2 over CNTs-3 can be explained by both the small specific surface area and the surface functional groups of CNTs-3. Generally, surface functional groups serve as anchoring sites for metal precursors, which will influence metal loading. However, it cannot be ignored that not all the anchoring of metal species is equally related to the functional groups. Therefore, it cannot be easily deduced that there exists a quantitative correlation between the metal loading and functional groups. Besides, the nitrogen functionalization can change the surface chemistry of the CNTs, e.g., hydrophobicity, polarity and proton affinity, which may influence the adsorption of the charged metal precursor in solution either.[41-42] Hence, all aspects should be taken into consideration.

Figure 5 (a) shows the XRD patterns of CZ/CNTs-3 with different treatment conditions during the preparation. As shown, both fresh and calcinated catalysts give the characteristic diffraction of (002) plane of graphite-like tube-wall of the CNTs at 2θ = 25.9° (JCPDS 26-1080);[22] the diffraction peaks located at 2θ = 35.6 and 38.8° can be ascribed to the diffraction of CuO (-111) and (111) planes, respectively (JCPDS 45-0937).[43] The wide diffraction peak in the range of 30.5～32.0° comes from the diffraction of amorphous ZrO_2 (JCPDS 37-1484), which is consistent with

the literatures that ZrO_2 will appear obvious crystallization after calcination above 500 °C.[44] Meanwhile, the calcinated catalyst shows stronger CuO and ZrO_2 diffraction peaks compared with the fresh catalyst, which is possibly due to the loss of crystallization water during the calcination, increasing the crystallinity of CuO and ZrO_2. After reduction, CuO feature diffraction peaks disappear while new diffraction peaks at 2θ = 43.1 and 50.1° are simultaneously observed. These two diffraction peaks can be attributed to the diffraction of elemental Cu (111) and (200) planes, respectively (JCPDS 65-9026).[43] The XRD patterns of CZ/CNTs-1 and CZ/CNTs-2 catalysts displayed similar trend as presented in supporting information (Figures S-4 and S-5, respectively).

Figure 5 (b) exhibits the XRD patterns of different catalysts after reduction in H_2. It is obvious that all catalysts have very similar diffraction features with only different diffraction intensity of Cu. Its diffraction intensity decrease in the following order: CZ/CNTs-1 > CZ/CNTs-2 > CZ/CNTs-3, especially for the diffraction of Cu (200) planes. The corresponding copper crystallite size was calculated through Scherrer equation and they are 21.1, 18.8 and 15.5 nm, respectively. Normally, the crystallinity and dispersion of Cu is in accordance with their copper crystallite size. Therefore, the dispersion of Cu increases in the order of CZ/CNTs-1, CZ/CNTs-2 and CZ/CNTs-3.

XPS results demonstrate that the oxygen content of CNTs-2 is much lower than that of CNTs-1, and negligible carboxyl groups were detected. Combined with XRD results that the crystal size of Cu particles on CZ/CNTs-2 after reduction is smaller than that of CZ/CNTs-1, it can be deduced that large amount of oxygen containing

functional groups, especially carboxylic acid group, may promote the growth of Cu on CNTs presumably due to its decomposition during heating/reduction in H_2, resulting in big Cu particle size. In contrast, the oxygen content of CNTs-3 is much higher than that of CNTs-2, while the crystal size of Cu particles on CZ/CNTs-3 is obviously smaller than that of CZ/CNTs-2. This means that nitrogen containing functional groups play vital roles on the high metal dispersion on CNTs. Chen et al.[29] observed the similar phenomena that Pd nanoparticles were stabilized on nitrogen-containing CNTs with narrower size distribution when compared with oxygen containing CNTs. Chen et al. [45] also disclosed that smaller Ru particle could be obtained on nitrogen doped CNTs than none-doped CNTs. This is presumably attributed to the existence of nitrogen atoms on the surface of CNTs, which increases the number of anchorage sites for the adsorption of the catalyst precursor salt, improving the nucleation of the active phase, preventing the surface mobility and then decreasing the probability of particle sintering during the thermal treatments.[46] Therefore, it can be concluded that large amount of acidic oxygen containing functional groups result in large Cu particle size while basic nitrogen containing functional groups are beneficial to the formation of small Cu particle size.

The H_2-TPR spectra of the calcinated catalysts are shown in Figure 6. Three reduction peaks can be revealed in all catalysts in the temperature range of 100-200 °C, this is in agreement with previous publication.[19] The low temperature reduction (120-150 °C) can be assigned to the amorphous or highly dispersed CuO reduction, or CuO species reduction to form Cu_2O then to metal copper species through gradual

reduction.[47,48] High temperature reduction (150-180 °C) can be assigned to bulk-like CuO phase reduction.[47,48] In addition, the reduction of other metal oxides was unobserved. The hydrogen consumption at different reduction stages is calculated by using the Gaussian function for TPR curve fitting, and the results are displayed in Table 4. Notably, the hydrogen consumption at low temperature reduction over these catalysts decreases in the following order: CZ/CNTs-3 ＞ CZ/CNTs-2 ＞ CZ/CNTs-1, with the corresponding hydrogen consumption of 0.596, 0.274 and 0.261mol_{H2}·mol_{Cu}^{-1}, respectively. As pointed out by Avgouropoulos et al.[49], smaller copper oxide particles are easier to be reduced, so the copper oxide particle size increase in the above order; this is in accordance with our XRD results. Furthermore, the reduction property of copper-based catalyst is affected by the interaction between copper oxide and the carrier.[11,49-50] Chew et al.[11] discovered that nanoparticles supported on nitrogen-functionalized CNTs were easier to be reduced compared to those on oxygen-functionalized CNTs. This promotion reduction effects was explained by the fact that the metal cations preferably locate on N-containing sites on the carbon surface, which favors the electron-donating from surface N species to metal oxide.[11,51] Besides, as expected large amount of low temperature reduction would inhibit the growth of metal Cu crystallite, resulting in high Cu dispersion.[19] These results indicate that CNTs with nitrogen species promote copper oxides reduction and contribute to small Cu particles formation; however, CNTs with oxygen species display negative effects on Cu dispersion.

The total hydrogen consumption sequence is consistent with that of their low temperature hydrogen consumption. For CZ/CNTs-3 catalyst, the total hydrogen consumptions is even little higher than 1 mol_{H2}·mol^{-1}Cu, which may be caused by the adsorption of H_2 on the surface of the catalysts. This further confirms that nitrogen-containing functional groups can promote the reduction of copper oxides. Hence, the presence of nitrogen species on CNTs result in large amount of highly dispersed Cu precursors and deep reduction of copper oxides. In summary, nitrogen-containing functional groups enhance the dispersion of copper oxides; promote their reduction, leading to small Cu crystal size.

Figure 7 Shows the H_2-TPD spectra of various catalysts. All catalysts contain a low temperature desorption peak spanning from 160 to 200 ^oC and a high temperature desorption peak located around 320 ^oC. Zhang et al. observed the similar H_2 desorption phenomena in their H_2-TPD study.[19] The former desorption can be ascribed to the desorption of dissociative adsorbed atomic hydrogen from the metallic Cu surface,[19,35,52] while the high temperature desorption represents the desorption of strongly adsorbed hydrogen on the bulk of Cu particles or the desorption from metal oxide surface[19,35,38,52]. As reported in the literature, pure ZrO_2 hardly adsorbs any hydrogen, but hydrogen can transport from Cu to ZrO_2 via spillover.[35,38,52] Thus, the total desorption amount of hydrogen from these sites reflects the dissociative adsorption capability of the catalysts. Then, the relative area-intensities of the two desorption peaks for these catalysts were calculated and listed in Table 5. The total amount of desorbed H_2 from the catalysts decrease in the

order: CZ/CNTs-3 ≥ CZ/CNTs-2 > CZ/CNTs-1. This trend agrees well with the Cu particle size. These results indicate that small Cu particles are favorable to the disassociation of H_2 and possess large H_2 disassociation capacity.

It is accepted that CO_2 hydrogenation on Cu/ZrO_2 interface follows a dual-site L-H mechanism; so many efforts have been made to carry out CO_2-TPD of the three catalysts.[53] However, surface functional groups decompose to release CO and CO_2 when rising temperature; moreover, metal can catalyze the decomposition.[27] Importantly, CNTs release more amounts of carbon oxides than adsorbed CO_2 at most time. Unfortunately, it cannot distinguish the carbon oxides desorption from CNTs or from adsorbed species on ZrO_2. Thus, it failed to get any useful information from CO_2-TPD of the investigated catalysts. Fortunately, CO_2-TPD of the supports were obtained and displayed in Figure 8. As shown, CNTs-3 exhibits obvious CO_2 desorption near 400 ^oC while CO_2 desorption from CNTs-1 and CNTs-2 were unobserved. This suggests that basic nitrogen containing functional groups can absorb CO_2.

Discussion

Since CO_2 hydrogenation to methanol is an exothermic reversible reaction, it is worthy to investigate the reaction behavior far away from the equilibrium (below 260 ^oC, here). Below 260 ^oC, both CO_2 conversion and CH_3OH selectivity decrease in the order of CZ/CNTs-3 > CZ/CNTs-2 > CZ/CNTs-1. Thus, the CH_3OH yield decreases in the same order. CO_2 hydrogenation to methanol on Cu/ZrO_2 interface follows a dual-site L-H mechanism through HCOO route,[35,53] involving hydrogenation and

basic oxide sites at the interfaces of metal and oxide phases. According to H_2- and CO_2-TPD analysis, the high CO_2 conversion observed on CZ/CNTs-3 may be due to the largest dissociative adsorption capacity of H_2 and CO_2 adsorption capability over CNTs-3, which mainly originates from nitrogen containing functional groups on CNTs surface.

Besides, previous publications reveal that the high CH_3OH selectivity may originate from the highly active Cu species and/or the properties of metal oxide supports/additives, such as γ basic site, the surface oxygen vacancies etc. [35,38,54-57] For example, Fujita et al.[54] believed that the CH_3OH selectivity is related to the preferential emergence of smooth surface Cu sites, such as Cu (100) and Cu (111). Toyir et al.[55] proposed that the active Cu^+ species enhanced CH_3OH selectivity and reduced CO selectivity. Jung et al.[56] put forward that the high concentration of methoxide species and formate intermediates on monoclinic zirconia contributed to the high CH_3OH selectivity. Guo et al.[35,38] revealed that CH_3OH selectivity is related to γ basic site on metal oxides. Wang et al.[57] attributed the high CH_3OH selectivity to the synergistic effect between CuO and the surface oxygen vacancies of doped ceria. Moreover, Zhang et al.[21,58] has proposed that the catalysts with high capacity for adsorption-activation of H_2 will increase the rate of surface hydrogenation reactions and CH_3OH selectivity. Therefore, combined the current research with the literature, here, the higher CH_3OH selectivity of CZ/CNTs-2 compared with CZ/CNTs-1 may be due to much larger dissociative adsorption capacity of hydrogen. The highest CH_3OH selectivity of CZ/CNTs-3 may originate from both the large hydrogen dissociative

adsorption capability and the CO_2 adsorption capability, compared with CZ/CNTs-1 and CZ/CNTs-2.

Conclusions

CNTs with basic and acidic surface functional groups supported Cu-ZrO_2 catalysts have been prepared by deposition-precipitation method and tested for CO_2 hydrogenation to methanol. CNTs, functionalized with nitrogen containing groups, supported Cu-ZrO_2 catalyst (CZ/CNT-3) demonstrated high intrinsic activity (turnover frequency $1.61x10^{-2}$ s^{-1}) and comparably high space time yield (84.0 $mg \cdot g^{-1}_{(cat)} \cdot h^{-1}$) with Cu loading level of only 10.3 wt% under the reaction conditions of 3.0 MPa, 260 °C, $V(H_2):V(CO_2):V(N_2)$ = 69:23:8, and GHSV = 3600 h^{-1}. The existence of nitrogen containing functional groups enhances the dispersion of Cu oxides, promotes their reduction, then results in small Cu crystal size, leading to high H_2 and CO_2 adsorption capability, finally high CO_2 conversion, CH_3OH selectivity and CH_3OH yield. The existence of acidic oxygen containing functional groups is responsible for negative effects on Cu dispersion, resulting in low CO_2 conversion, finally low CH_3OH yield.

Acknowledgements

This work is financially supported by the National Natural Science Foundation of China (No. 21207039, 51108187, U1201231), the Natural Science Foundation of Guangdong Province, China (Grant No. S2011010000737), Specialized Research Fund for the Doctoral Program of Higher Education, China (20110172120017), and

Scientific Research Foundation for Returned Scholars, Ministry of Education of China (2012).

Reference

1 I. Ganesh, Renew. *Sus. Energy Rev.*, 2014, **31**, 221-257.

2 G. Centi, G. Iaquaniello and S.Perathoner, *ChemSusChem*, 2011, **4**, 1265-1273.

3 G. Centi, E. A. Quadrelli and S. Perathoner, *Energy Environ. Sci.*, 2013, **6**, 1711-1731.

4 E. V. Kondratenko, G. Mul, J. Baltrusaitis, G. O. Larrazábal and J. Pérez-Ramírez, *Energy Environ. Sci.*, 2013, **6**, 3112-3135.

5 Y. Izumi, *Coordination Chem. Rev.*, 2013, **257**, 171-186.

6 N. A. M. Razali, K. T. Lee, S. Bhatia and A. R. Mohamed, *Renew. Sus. Energy Rev.*, 2012, **16**, 4951-4964.

7 W. Wang, S. Wang, X. Ma and J. L. Gong, *Chem. Soc. Rev.*, 2011, **40**, 3703-3727.

8 X. M. Guo, D. S. Mao, G. Z. Lu, S. Wang and G. S. Wu, *J. Catal.*, 2010, **271**, 178-185.

9 X. M. Liu, G. Q. Lu, Z. F. Yan and J. Beltramini, *Ind. Eng. Chem. Res.*, 2003, **42**, 6518-6530.

10 G. A. Olah, A. Goeppert and G. K. S. Prakash, *Beyond oil and gas: The Methanol Economy*, 2nd ed., Wiley-VCH, Weinheim, 2009.

11 L. M. Chew, P. Kangvansura and H. Ruland, *Appl. Catal. A*, 2014, **482**, 163-170.

12 A. Bansode and A. Urakawa, *J. Catal.*, 2014, **309**, 66-70.

13 F. Arena, G. Mezzatesta, G. Zafarana, G. Trunfio, F. Frusteri and L. Spadaro, *J. Catal.,* 2013, **300**, 141-151.

14 G. Bonura, M. Cordaro, C. Cannilla, F. Arena and F. Frusteri, *Appl. Catal. B*, 2014, **152-153**, 152-161.

15 E. Frei, A. Schaadt, T. Ludwig, H. Hillebrecht and I. Krossing, *ChemCatChem*, 2014, **6**, 1721-1730.

16 Y. Hartadi, D. Widmann and R. J. Behm, *ChemSusChem*, 2015, **8**, 456-465.

17 M. Kilo, J. Weigel, A. Wokaun, R. A. Koeppel, A. Stoeckli and A. J. Baiker, *J. Mol. Catal. A*, 1997, **126**, 169-184.

18 S. B. Xie, E. Iglesia and A. T. Bell, *Chem. Mater.*, 2000, **12**, 2442-2447.

19 X. Dong, H. B. Zhang, G. D. Lin, Y. Z. Yuan and K. R. Tsai, *Catal. Lett.*, 2003, **85**, 237-246.

20 X. Dong, X. L. Liang, H. Y. Li, G. D. Lin, P. Zhang and H. B. Zhang, *Catal. Today*, 2009, **147**, 158-165.

21 H. B. Zhang, X. L. Liang, X. Dong, H. Y. Li and G. D. Lin, *Catal. Sur. Asia*, 2009, **13**, 41-58.

22 X. L. Liang, X. Dong, G. D. Lin and H. B. Zhang, *Appl. Catal. B*, 2009, **88**, 315-322.

23 Z. Q. Yang, S. J. Guo, X. L. Pan, J. H. Wang and X. H. Bao, *Energy Environ. Sci.*, 2011, **4**, 4500-4503.

24 X. L. Pan and X. H. Bao, *Accounts Chem. Res.*, 2011, **44**, 553-562.

25 L. M. Chen, D. Ma, Z. Zhang, Y. Y. Guo, D. Q. Ye and B. C. Huang, *ChemCatChem*, 2012, **4**, 1960-1967.

26 L. M. Chen, D. Ma, Z. Zhang, Y. Y. Guo, D. Q. Ye and B. C. Huang, *Catal. Lett.*, 2012, **142**, 975-983.

27 L. M. Chen, D. Ma and X. H. Bao, *J. Phys. Chem. C*, 2007, **111**, 2229-2234.

28 Y. C. Chiang, W. H. Lin and Y. C. Chang, *Appl. Sur. Sci.*, 2011, **257**, 2401-2410.

29 J. L. Chen, Q. H. Chen, Q. Ma, Y. D. Li and Z. H. Zhu, *J. Mol. Cat. A*, 2012, **356**, 114-120.

30 L. J. Jia, D. A. Bulushev and O. Y. Podyacheva, *J. Catal.*, 2013, **307**, 94-102.

31 P. R. Chen, F. K. Yang, A. Kostka and W. Xia, *ACS Catal.*, 2014, **4**, 1478-1486.

32 F. Arena, K. Barbera, G. Italiano, G. Bonura, L. Spadaro and F. Frusteri, *J. Catal.*, 2007, **249**, 185-194.

33 J. Y. Liu, J. L. Shi, D. H. He, Q. J. Zhang, X. H. Wu, Y. Liang and Q. M. Zhu, *Appl. Catal. A*, 2001, **218**, 113-119.

34 M. Kilo, J. Weigel, A. Wokaun, R. A. Koeppel, A. Stoeckli and A. Baiker, *J. Mol. Catal. A*, 1997, **126**, 169-184.

35 X. M. Guo, D. S. Mao, G. Z. Lu, S. Wang and G. S. Wu, *J. Mol. Catal. A*, 2011, **345**, 60-68.

36 X. M. Liu, G.Q. Lu and Z. F. Yan, *Appl. Catal. A*, 2005, **279**, 241-245.

37 J. Słoczyński, R. Grabowski, A. Kozłowska, P. Olszewski, J. Stoch, J. Skrzypek and M. Lachowsk, *Appl. Catal. A*, 2004, **278**, 11-23.

38 X. M. Guo, D. S. Mao, G. Z. Lu, S. Wang and G. S. Wu, *J. Catal.*, 2010, **271**, 178-185.

39 X. M. Guo, D. S. Mao, G. Z. Lu, S. Wang and G. S. Wu, *Catal. Commun.*, 2011, **12**, 1095-1098.

40 Y. Ma, Q. Sun, D. Wu, W. H. Fan, Y. L. Zhang and J. F. Deng, *Appl. Catal. A*, 1998, **171**, 45-55.

41 R. Arrigo, M. Hävecker, S. Wrabetz, R. Blume, M. Lerch, J. McGregor, E. P. J. Parrott, J. A. Zeitler, L. F. Gladden, A. Knop-Gericke, R. Schlögl and D. S. Su, *J. Am. Chem. Soc.*, 2010, **132**, 9616-9630.

42 D. J. Suh and T. Park, *Carbon*, 1993, **31**, 427-435.

43 C. M. Li, X. D. Yuan and K. Fujimoto, *Appl. Catal. A*, 2014, **469**, 306-311.

44 S. Esposito, M. Turco, G. Bagnasco, C. Cammarano, P. Pernice and A. Aronne, *Appl. Catal. A*, 2010, **372**, 48-57.

45 J. L. Chen, Z. H. Zhu and S. B. Wang, *Chem. Eng. J.*, 2010, **156**, 404–410.

46 K. Chizari, A. Deneuve, O. Ersen, I. Floreab, Y. Liu, D. Edouard, I. Janowska, D. Begin and C. Pham-Huu. *Appl. Catal. A-Gen.,* 2010, **380**, 72-80.

47 S. D. Jones and H. E. Hagelin-Weaver, *Appl. Catal. B*, 2009, **90**, 195-204.

48 G. Aguila, J. Jimenez, S. Guerrero, F. Gracia, B. Chornik, S. Quinteros and P. Araya, *Appl. Catal. A*, 2009, **360**, 98-105.

49 G. Avgouropoulos and T. Ioannides, *Appl. Catal. A*, 2003, **244**, 155-167.

50 G. Avgouropoulos, T. Ioannides and H. Matralis, *Appl. Catal. B*, 2005, **56**, 87-93.

51 S. Pylypenko, A. Borisevich, K. L. More, A. R. Corpuz, T. Holme, A. A. Dameron, T. S. Olson, H. N. Dinh, T. Gennett and R. O'Hayre, *Energy Environ. Sci.*, 2013, **6**, 2957-2964.

52 F. Arena, G. Italiano, K. Barbera, S. Bordiga, G. Bonura, L. Spadaro and F. Frusteri, *Appl. Catal. A*, 2008, **350**, 16-23.

53 Q. J. Hong and Z. P. Liu, *Surf. Sci.*, 2010, **604**, 1869-1876.

54 S. Fujita, S. Moribe, Y. Kanamori, M. Kakudate and N. Takezawa, *Appl. Catal. A*, 2001, **207**, 121-128.

55 J. Toyir, P. R. de la Piscina, J. L. G. Fierro and N. Homs, *Appl. Catal. B*, 2001, **34**, 255-266.

56 K. T. Jung and A. T. Bell, *Catal. Lett.*, 2002, **80**, 1-2.

57 J. B. Wang, H. K. Lee and T. J. Huang, *Catal. Lett.*, 2002, **83**, 79-86.

58 H. B. Zhang, X. Dong, G. D. Lin, X. L. Liang and H. Y. Li, *Chem. Commun.*, 2005, **40**, 5094-5096.

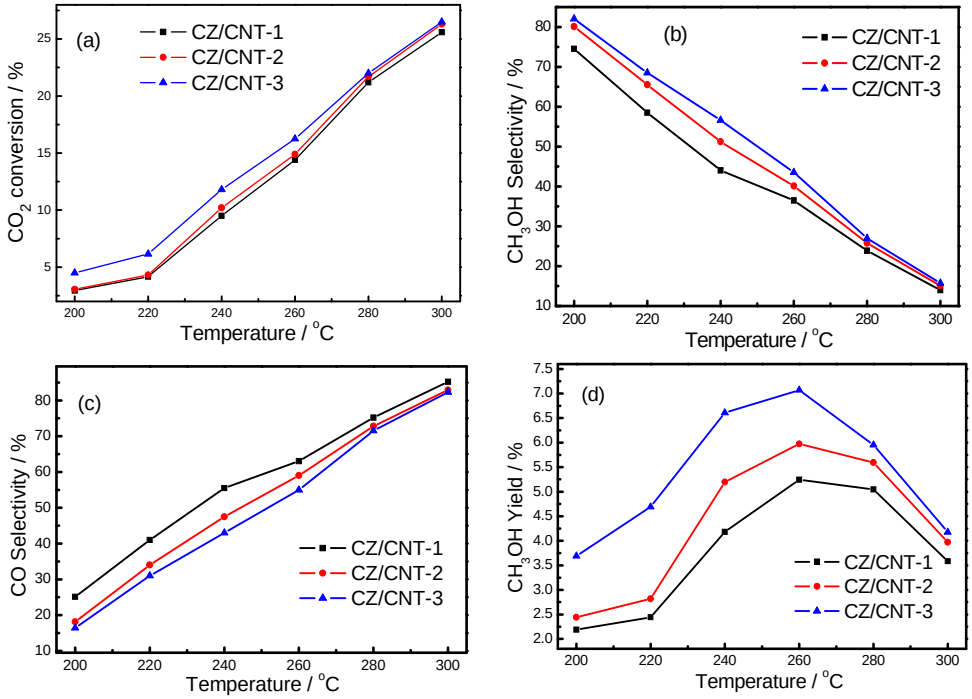

Fig. 1 The (a) CO_2 Conversion, (b) CH_3OH Selectivity, (c) CO Selectivity and (d) CH_3OH yield over the catalysts at different reaction temperatures. Reaction conditions: $V(H_2):V(CO_2):V(N_2) = 69:23:8$, $p = 3.0$ MPa, GHSV = 3600 $mL \cdot g_{cat}^{-1} \cdot h^{-1}$.

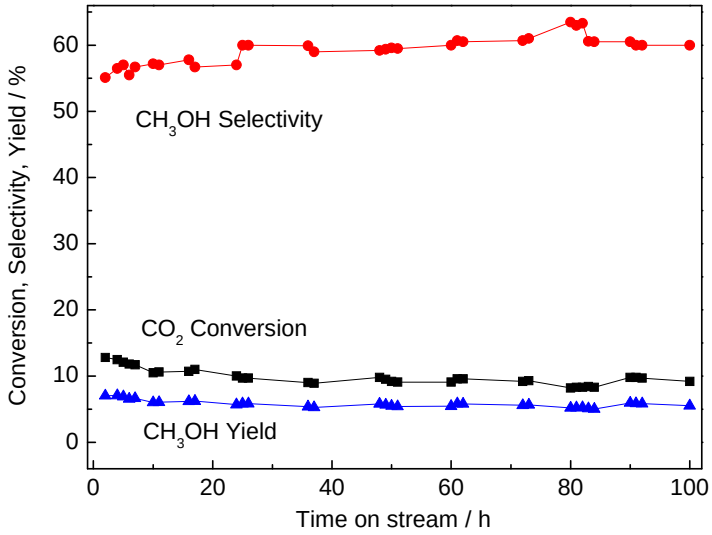

Fig. 2 Variation of CO_2 conversion, CH_3OH selectivity and yield with reaction time over CZ/CNTs-3. Reaction conditions: $V(H_2):V(CO_2):V(N_2)$ = 69:23:8, p = 3.0 MPa, GHSV = 3600 $mL \cdot g_{cat}^{-1} \cdot h^{-1}$.

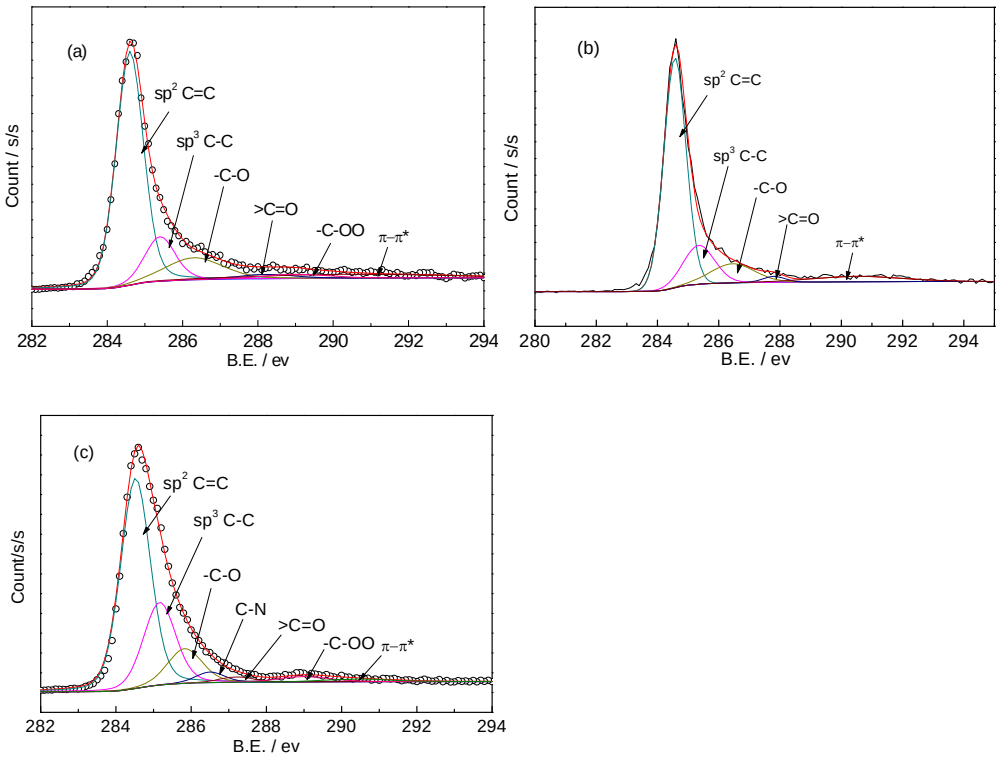

Fig. 3 High resolution XPS C1s spectra of (a) CNTs-1, (b) CNTs-2 and (c) CNTs-3.

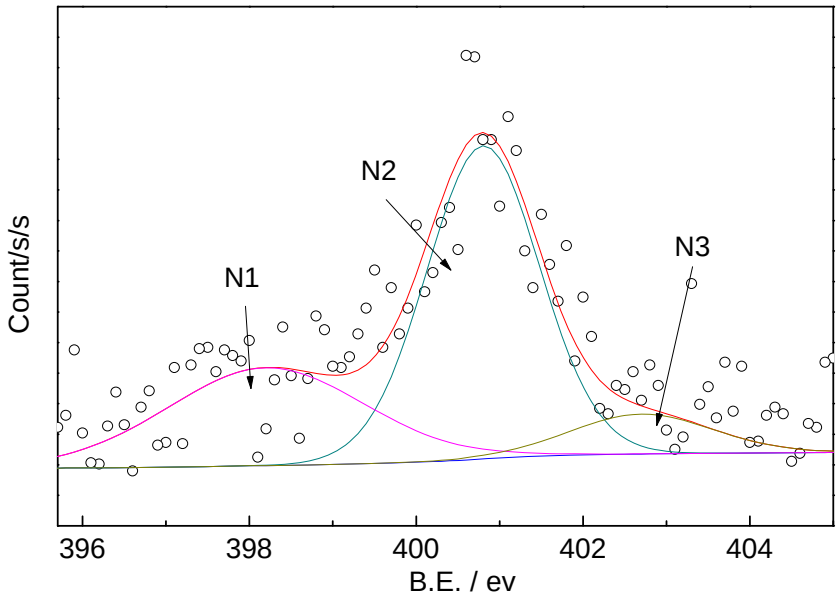

Fig. 4 High resolution XPS N1s spectra of CNTs-3.

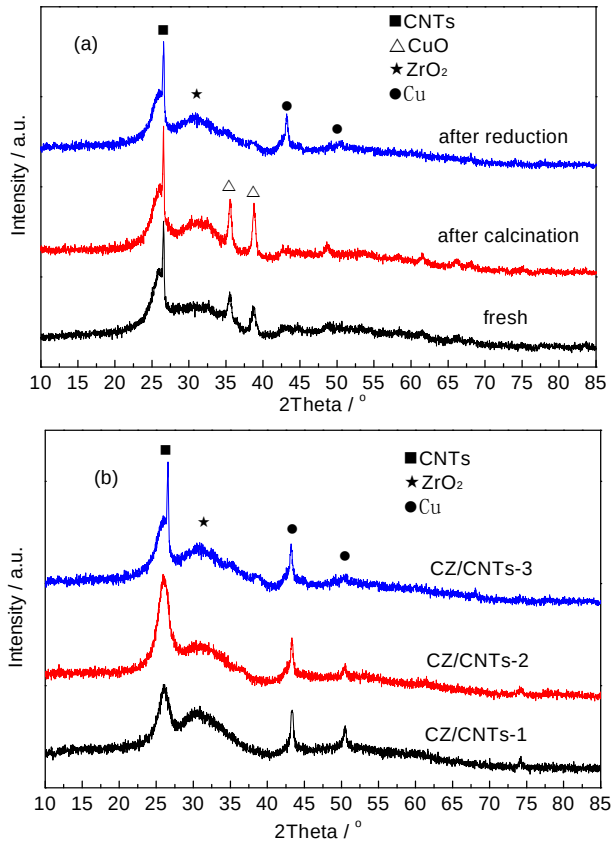

Fig. 5 XRD patterns of (a) CZ/CNTs-3 after different treatment conditions, and (b) different catalysts after reduction in H_2.

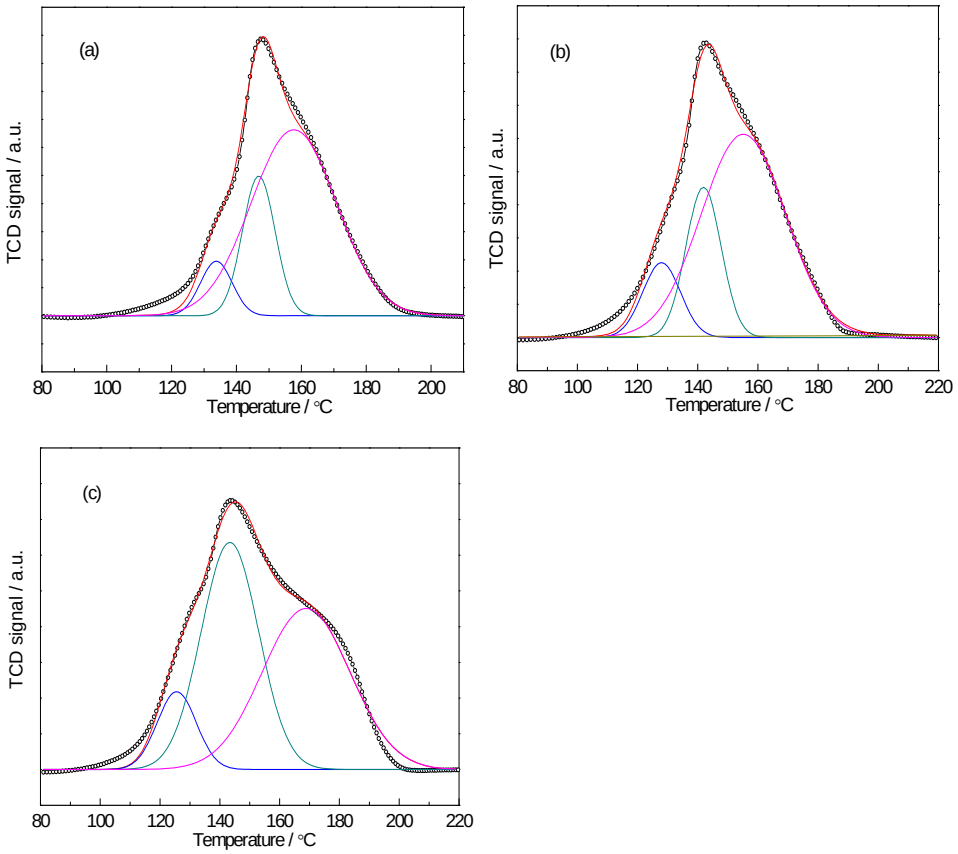

Fig. 6 H_2-TPR profiles of the calcinated (a) CZ/CNTs-1, (b) CZ/CNTs-2 and (c) CZ/CNTs-3 catalyst.

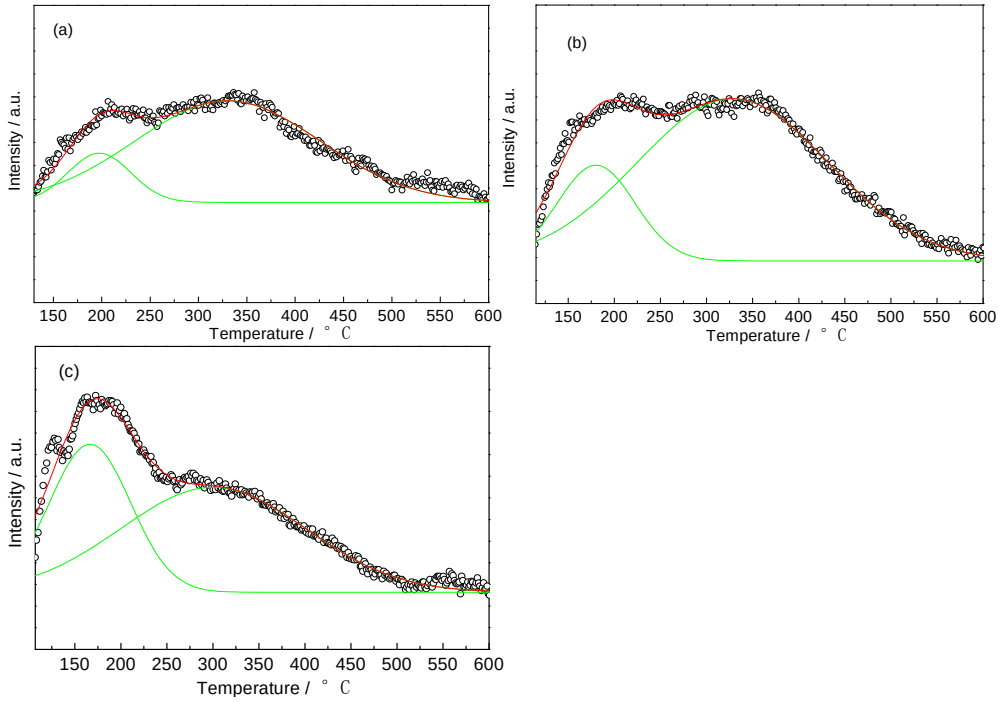

Fig. 7 H_2-TPD profiles of the reduced (a) CZ/CNTs-1, (b) CZ/CNTs-2 and (c) CZ/CNTs-3 catalyst.

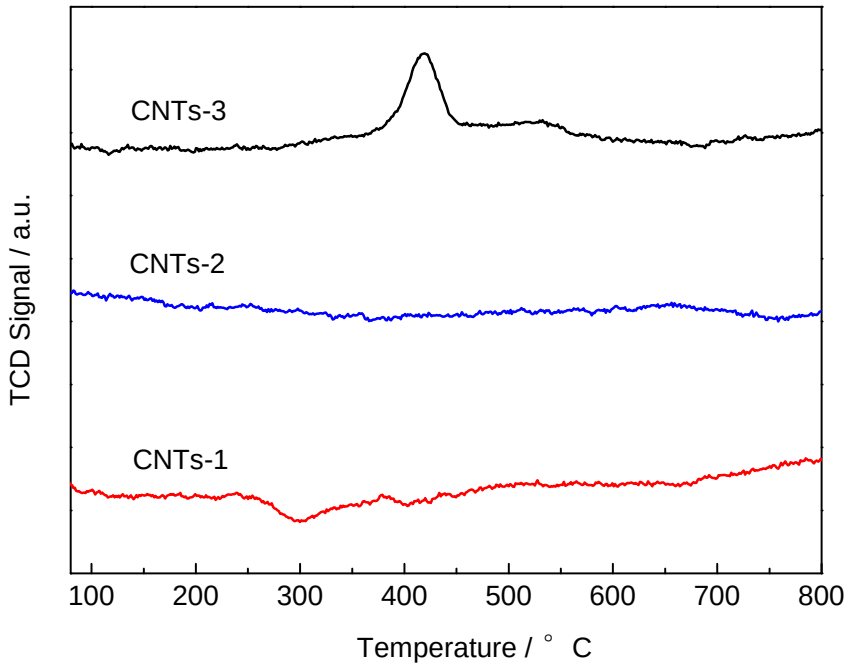

Fig. 8 CO_2-TPD profiles of different CNT supports.

Table 1 Methanol synthesis from CO_2 hydrogenation over various catalysts

Catalyst [a]	T[°C], P[MPa], GHSV[h^{-1}]	CO_2 Conv. [%]	CH_3OH Selec. [%]	CH_3OH Yield [%]	d_{Cu} [nm]	TOF $*10^2$ [s^{-1}]	STY [$mg \cdot g^{-1}h^{-1}$]	Ref.
CZ/CNTs-1	220,3.0,3600	4.1	58.5	2.44	21.1	0.45	28.9	-
CZ/CNTs-2	220,3.0,3600	4.3	65.5	2.82	18.8	0.43	33.4	-
CZ/CNTs-3	220,3.0,3600	6.9	68.5	4.69	15.5	0.68	55.5	-
CZ/CNTs-1	240,3.0,3600	9.5	44.0	4.18	21.1	1.03	49.4	-
CZ/CNTs-2	240,3.0,3600	10.2	51.2	5.22	18.8	1.02	61.8	-
CZ/CNTs-3	240,3.0,3600	11.1	54.0	5.96	15.5	1.09	70.5	-
CZ/CNTs-1	260,3.0,3600	14.4	36.5	5.26	21.1	1.56	62.2	-
CZ/CNTs-2	260,3.0,3600	14.9	40.1	5.97	18.8	1.50	70.7	-
CZ/CNTs-3	260,3.0,3600	16.3	43.5	7.09	15.5	1.61	83.9	-
$CuO_{(58.6)}/ZrO_{2(41.4)}$	240,3.0,4400	17.6	48.8	8.59	32	0.97	124.7	[32]
$CuO_{(30)}/ZrO_{2(70)}$	240,2.0,5400	6.3	48.8	3.07	16	0.45	59.3	[33]
$Cu_{(18.2)}/ZrO_{2(81.8)}$	220.1.7,5400	4.4	77.0	3.39	19	0.49	65.3	[34]
$Cu_{(31.5)}/La_2O_{3(8.0)}/ZrO_{2(60.5)}$	220,3.0,3600	6.2	66.0	4.09	48.4[b]	0.60	46.3	[35]
$Cu_{(27)}/B_2O_{3(3)}/ZrO_{2(70)}$	250,2.0,2500	15.8	67.3	10.63			94.9	[36]
$Cu_{(27)}/Ga_2O_{3(3)}/ZrO_{2(70)}$	250,2.0,2500	13.7	75.6	10.36			92.5	[36]
$Cu_{(6.7)}/ ZnO_{(64.4)}/ZrO_{2(28.9)}$	220.8.0,3300	9.0	75.0	6.75	9.8	0.86	79.6	[37]
$CuO_{(43)}/ZnO_{(17.4)}/ZrO_{2(39.6)}$	220,3.0,3600	12.0	71.1	8.53		1.65[c]	109.7	[38]
$CuO_{(43)}/ZnO_{(17.4)}/ZrO_{2(39.6)}$	240,3.0,3600	15.7	58.0	9.11	18.2[b]	0.62	117.1	[39]
$Cu_{(37.0)}/ZnO_{(47.2)}/ZrO_{2(15.8)}$	250,2.0,3600	18.7	36.7	6.9	15.7	0.57	88.2	[40]

[a] The catalysts are labeled by mass ratio. [b] The particle size is calculated through the dispersion of Cu. [c] TOF is calculated through the reference [38].

Table 2 The relative amount of different carbon species from the XPS C1s region and CNT surface composition from XPS (at%)

Sample	Binding energy (eV)				O	N	C
	285.9-286.5 C-OH[a]	286.7 C-N[a]	287.4-288 C=O[a]	289 -COOH[a]	[at%]		
CNTs-1	12.4	-	2.38	2.62	7.03	-	92.97
CNTs-2	10.7	-	1.67	-	1.89	-	98.11
CNTs-3	10.9	2.73	1.58	2.48	5.76	0.84	93.4

[a] The amount of oxygen or nitrogen functionalized carbon species / total amount of carbon.

Table 3 Characteristics of the investigated CNTs and the composition of the corresponding catalysts.

Sample	S_{BET} [$m^2 \cdot g^{-1}$]	V_{Total} [$cm^3 \cdot g^{-1}$]	Pore size distribution [nm]	Cu [wt%]	ZrO_2 [wt%]
CNTs-1	184	0.55	3.0	-	-
CNTs-2	193	0.60	2.1-3.0	-	-
CNTs-3	160	0.41	2.7	-	-
CZ/CNTs-1	156	0.33	2.6	12.8	35.8
CZ/CNTs-2	161	0.41	2.2	12.3	35.1
CZ/CNTs-3	128	0.31	2.3	10.3	32.7

Table 4 TPR data of the calcinated catalysts (T, ^{o}C; $n_{H2/Cu}$, $mol_{H2}\cdot mol_{Cu}^{-1}$)

Catalyst	$T_{M1/}$ T_{M2}[a]	$n_{H2/Cu}$[a]	T_{M3}[a]	$n_{H2/Cu}$[b]	$n_{H2/Cu}$[c]
CZ/CNTs-1	134/147	0.261	158	0.660	0.921
CZ/CNTs-2	126/142	0.274	155	0.662	0.936
CZ/CNTs-3	124/143	0.596	170	0.484	1.080

[a] Temperature of the peak maxima. [b] Hydrogen consumption amount during the first two reduction process. [c] Total hydrogen consumption amount

Table 5 Relative area-intensity of H_2-TPD peaks I and II for the reduced catalysts

Catalyst	T_α [^oC]	Relative area-intensity [a]	T_β [^oC]	Relative area-intensity [a]	Total relative area-intensity [a]
CZ/CNTs-1	198	14.3	330	68.0	82.3
CZ/CNTs-2	180	21.0	328	100	121
CZ/CNTs-3	166	61.2	300	65.1	126.3

[a] The area-intensity of the strongest peak β was set as 100.